Photocatalytic Activity of Neodymium Ion-doped TiO_2 for 2-Mercaptobenzothiazole Degradation under Visible Light Irradiation

F. B. Li[A, B], X. Z. Li[A,D] and K. W. Cheah[C]

[A] Department of Civil and Structural Engineering, The Hong Kong Polytechnic University, Hong Kong, China.

[B] Guangdong Key Laboratory of Agricultural Environment Pollution Integrated Control, Guangdong Institute of Eco-Environment and Soil Science, Guangzhou, 510650, China.

[C] Department of Physics, Hong Kong Baptist University, Hong Kong, China.

[D] *Corresponding author. Email: cexzli@polyu.edu.hk*

Environmental Context. Lanthanide ions with their $4f^n$ electronic-level structure are excellent luminescent materials. Conventional titanium dioxide catalyst modified by doping with lanthanide ions can conduct photocatalytic oxidation reaction under visible light irradiation in aqueous environment.

Abstract. A series of neodymium ion-doped titanium dioxide (Nd^{3+}-TiO_2) catalysts were prepared by a sol-gel method. The physical and chemical properties of the catalysts were characterized by X-ray diffraction (XRD), Brunauer-Emmett-Teller (BET) method, UV-visible diffusive reflective spectroscopy (DRS), and Photoluminescence (PL) analyses. The adsorption behaviour and photocatalytic activity of Nd^{3+}-TiO_2 under visible light irradiation were evaluated in aqueous 2-mercaptobenzothiazole (MBT) solution. The analytical results of XRD and BET demonstrate that the neodymium ion doping could reduce the crystallite size and increase the specific surface area of TiO_2 catalysts. The analytical results of DRS show that neodymium ion doping did not shift the main absorption band edge significantly, but some new absorption peaks attributable to 4*f* internal electron transition existed in the visible region. It was further confirmed that significant PL emission occurred in the visible range of 350-700 nm, attributable to the electron transfer between Nd^{3+} and TiO_2 owing to introduction of a Nd 4*f* level. The experimental results of adsorption isotherm tests demonstrate that both the saturated adsorption amount (Γ_{max}) and adsorption equilibrium constant (K_a) of Nd^{3+}-TiO_2 catalysts increased significantly with the increase of neodymium ion dosage. Furthermore, the Nd^{3+}-TiO_2 catalysts demonstrated the significant activity of photocatalytic degradation of MBT in aqueous solution under visible light irradiation, while the TiO_2 catalyst did not. An optimal dosage of neodymium ion doping was found to be 0.7%. It might be proposed that the introduction of the Nd 4*f* level plays a crucial role in visible photosensitization and enhancement of the electron-hole pair's separation.

Keywords: Neodymium ion - Nd^{3+} - Photocatalysis - 2-mercaptobenzothiazole - Titanium dioxide - TiO_2 - Visible light

Introduction

2-mercaptobenzothiazole (MBT) is known as a widespread, toxic, and poorly biodegradable pollutant in our environment. MBT and its derivatives are normally used as a bio-corrosion inhibitor or anti-fungal drug in medical applications, a coating agent of metallic surfaces and also a vulcanization accelerator in rubber industry [1]. In aquatic environment, the MBT has been detected in wastewater effluents from rubber additive manufacturers, tanneries, and often found in wastewater treatment plant and surface water [2]. The MBT can be transformed into benzothiazole (BT) in anaerobic media, and into 2-hydroxy benzothiazole (OBT) and benzothiazole-2-sulfonate ($BTSO_3$) in aerobic conditions. Consequently, MBT, BT, OBT, and $BTSO_3$ are frequently found in both of wastewater and surface water. These semi-volatile organic compounds also result in some odour problems in wastewater treatment plants [2]. Habibi et al [3] investigated the photocatalytic oxidation of 5 kinds of mercaptans including MBT and found that they could be almost completely mineralized to carbon dioxide and sulphate ion.

Titanium dioxide (TiO_2) has been paid much attention to its application potential due to the complete mineralization of toxic and nonbiodegradable organic contaminants into CO_2, H_2O and harmless inorganic products.[4] However, pure TiO_2 can only be excited by UV light with a wavelength of less than 387 nm. It had been extensively reported that doping/implanting/depositing with a group of transitional metal ions [5-7] or noble metals [8] with *d* electronic configuration into TiO_2 lattice or non-metal elements (N [9-10], B [11] and S [12]), or coupling metal oxides [13-17] could result in extension of their wavelength response into the visible light region**.** Alternatively, TiO_2-based photocatalysts would have visible light activity by doping with lanthanide ions/oxides with $4f^n$ electron configuration.[18, 19]

Lanthanide ions are excellent luminescent materials as guests because the $4f^n$ electronic-level structure of rare-earth ions possess certain long-lived intermediate levels and electrons could be excited with higher frequency photons to these metastable levels, where strong visible wavelength emission takes place.[20] It has been proven that TiO_2 is an ideal host matrix with strong optical absorption and efficient energy transfer to lanthanide ions, and is stable to environmental conditions. The ground states of most lanthanide ions lie below the valence band of metal oxides including TiO_2.[21] Frindell et al.[22] confirmed the efficient energy transfer from titania to the europium ions. Hwang et al.,[23] Machida et al.,[24, 25] and Zou et al.[26] reported that the photocatalytic activity of perovskite photocatalysts such as $Ln_2Ti_2O_7$, $MLnTa_2O_7$, $LnTaO_4$, and $BiRNbO_7$ for overall water splitting depends strongly on Ln 4*f* level. Among all lanthanide ions,

neodymium (Nd) is an interesting element, because the filled Nd $4f^4$ levels should lie within the O $2p$ valence band and the O $2p$ orbital can be hybridized with Nd $4f^4$ orbital. The interaction between Nd $4f$ and O $2p$ would be decisive to the electron transfer and then photocatalytic activity. These studies indicate that the optical properties and photocatalytic properties of neodymium ion-doped TiO_2 catalysts should be significantly affected by the host $4f^4$ level.

In this study, a series of neodymium ion-doped titanium dioxide (Nd^{3+}-TiO_2) catalysts were prepared by doping Nd^{3+} into TiO_2 and attention has been paid to their optical properties due to the electronic structure of $4f^45d^0$. The photocatalytic activity of the prepared Nd^{3+}-TiO_2 catalysts under visible light irradiation was investigated in the photocatalytic degradation of MBT in aqueous solution.

Experimental Methods

Preparation of Nd^{3+}-TiO_2 Catalysts

A series of Nd^{3+}-TiO_2 catalysts were prepared by a sol-gel method. In which 17 mL of tetra-n-butyl titanium ($Ti(O\text{-}Bu)_4$) dissolved in absolute ethanol was added drop-wise under vigorous stirring into 100 mL of a mixture solution containing 84 mL of ethanol (95%), 1 mL of 0.1 M $Nd(NO_3)_3$ solution and 15 mL of acetic acid (99.8%). The resulting transparent colloidal suspension was stirred for 2 h and then aged for 2 d till the formation of gel. The gel was dried at 353 K under vacuum, ground, and then sintered at 773 K for 2 h. Eventually the Nd^{3+}-TiO_2 powder was obtained in a nominal atomic doping level of 0.2% named 0.2% Nd^{3+}-TiO_2. In the meantime, other Nd^{3+}-TiO_2 samples were also prepared according to the above procedure as 0.7% Nd^{3+}-TiO_2, 1.2% Nd^{3+}-TiO_2, and 2.0% Nd^{3+}-TiO_2. All chemicals with analytical grade and deionized distilled water were used in solution preparation.

Characterization of Nd^{3+}-TiO_2 Catalysts

To determine the crystal phase composition of the prepared Nd^{3+}-TiO_2 samples, X-ray diffraction (XRD) measurement was carried out at room temperature using a Rigaku D/MAX-IIIA diffractometer with CuK_α radiation (λ = 0.15418 nm). The accelerating voltage of 30 kV and emission current of 30 mA were applied. The specific surface areas of all samples were measured by the Brunauer-Emmett-Teller (BET) method, in which a N_2 gas was adsorbed at 77 K using a Carlo Erba sorptometer. To study the light absorption of the photocatalysts, the samples were examined using a spectrophotometer (Perkin Elmer UVW-340) and the diffuse reflectance spectroscopy (DRS) in the range of 200-800 nm were applied, while $BaSO_4$ was used as a reference. To study the recombination between electrons and holes within the catalysts, the photoluminescence (PL) emission spectra of the samples were measured in the following procedure: at 77 K and room temperature, a 325 nm He-Cd laser was used as an excitation light source; The

light from the sample was focused into a spectrometer (Spex500) and detected by a photomultiplier tube (PMT); The signal from the PMT was input to a photon counter (SR400) before recorded by a computer.

MBT Adsorption Isotherm

MBT (2-mercaptobenzothiazole) was provided by BDH and used as a model chemical in this study without further purification. To determine the adsorption behaviour of Nd^{3+}-TiO_2 catalysts, a set of adsorption isotherm tests was performed in the dark, in which the 10 mL of MBT solutions with different concentrations were added with 0.1 g of Nd^{3+}-TiO_2 catalysts and then the suspensions were put into a shaker operated at 130 rpm for 24 h at room temperature. The MBT concentration in the suspensions before and after the adsorption tests was analysed to determine the adsorbed amount of MBT on the catalysts from a mass balance.

Experimental Setup and Procedures

A Pyrex cylindrical photoreactor was used in the experiments to conduct photocatalytic oxidation experiments, in which a 110-W high-pressure sodium lamp with main emission in the range of 400-800 nm was used for photoreaction under visible light irradiation. The minor portion of UV emission from the sodium lamp was filtered by 0.5 M $NaNO_2$ solution with a cut-off wavelength of 400 nm. This photoreactor was surrounded by a Pyrex circulating water jacket to control the temperature during the reaction. The reaction suspension was prepared by adding 0.25 g of photocatalyst powder into 250 mL of aqueous MBT solution. Prior to photoreaction, the suspension was magnetically stirred in a dark condition for 30 min to establish adsorption/desorption equilibrium. The aqueous suspension containing MBT and photocatalyst was irradiated under visible illumination with constant aeration. At the given time intervals, the water samples were taken from the suspension and immediately centrifuged at 60 rps for 20 min, then filtered through a 0.45-μm Millipore filter to remove the particles. The filtrate was analysed as required.

Analytical Methods

The MBT remaining during the photodegradation was determined by liquid chromatography (LC), which consists of a gradient pump (Spectra System P4000), an autosampler (Spectra System Tem AS3000) with a 20-μl injection loop, a Thermo Ques Hypersil ODS column (C18, 5 μm, 250 × 4.6 mm ID) and a photodiode array UV detector (Spectra SYSTEM UV6000LP). While a mobile phase consisting of 70% methanol (HPLC grade) and 30% water (HPLC grade) acidified by adding 1% (v/v) acetic acid was operated at a flow rate of 0.5 mL min^{-1}, a wavelength of 323 nm was used to detect MBT. Dissolved organic carbon (DOC) was determined by a total organic carbon (TOC)

analyser (Shimadzu 5000A) equipped with an autosampler (ASI-5000). The final products including sulphate ion, nitrate ion and ammonium ion from the MBT photocatalytic degradation were determined by ion chromatography with a conductivity detector (Shimadzu HIC-6A), in which a Shim-Pack IC-A1 anion column and the mobile phase containing 2.5 mM phthalic acid and 2.4 mM tris(hydroxymethyl)-aminomethane were used at a flow rate of 1.5 mL min^{-1} for determination of sulphate and nitrate ion, while a Shim-Pack IC-C1 cationic column and the mobile phase containing 5.0 mM nitrate acid were used at a flow rate of 1.0 mL min^{-1} for determination of ammonium ion.

Results and discussion

Dark Adsorption

To determine the adsorption capacity of different catalysts, a set of adsorption tests was carried out in the dark. The MBT adsorption isotherms on the catalysts are shown in Fig. 1 by plotting Γ vs. C_e, in which the saturated adsorption amount (Γ_{max}) and the adsorption equilibrium constant (K_a) were calculated by the Langmuir adsorption model [27] and the fitting results are listed in Table 1. The results confirmed that all Nd^{3+}-TiO_2 samples had better adsorption ability than the TiO_2 sample. While the saturated adsorption amount (Γ_{max}) of TiO_2 was 8.91×10^{-6} mol g^{-1}, that of Nd^{3+}-TiO_2 increased with the increase of neodymium ion dosage up to 14.1×10^{-6} mol g^{-1}. The results also indicate that the adsorption equilibrium constants (K_a) of Nd^{3+}-TiO_2 are about twice of TiO_2. The factors leading to the enhanced adsorption capacity involve the change of physical or chemical properties of the catalysts owing to neodymium ion doping. Firstly the larger specific surface area of the Nd^{3+}-TiO_2 catalysts as shown in Table 2 would be beneficial to achieve better physical adsorption to MBT in the aqueous suspensions. Secondly there might be formation of a chemical complex between Nd^{3+} with $4f^0$ empty orbital and the -SH group of MBT. Although the complex of Ti^{4+}-SH could also be formed because of Ti^{4+} with $3d^0$ empty orbital, the equilibrium constant for the formation of Ti^{4+}-SH is much lower than that of Nd^{3+}-SH. It was reported that lanthanide ions could form complexes with various Lewis bases including organic acids, amines, aldehydes, alcohols, and thiols in the interaction of the functional groups with their full empty or partial empty 4*f*-orbitals.[28]

[Fig. 1]

[Table 1]

Photocatalytic Activity under Visible Light Irradiation

To evaluate the photocatalytic activity of Nd^{3+}-TiO_2 catalysts under visible light irradiation, a set of tests was carried out to degrade MBT in aqueous suspension with an initial MBT concentration of 0.13 mM. Since we have obtained K_a values of Nd^{3+}-TiO_2 catalysts in the adsorption tests, the apparent kinetic constant (K_{ap}) of MBT photodegradation using different TiO_2 catalysts can be calculated by using the following integral form of the Langmuir-Hinshelwood (L-H) model based on the experimental data.

$$Ln(C_0/C) + K_a \cdot (C_0 - C) = k_{ap} \cdot t \quad (1)$$

where $k_{ap} = k_r \cdot K_a$, is the apparent kinetic constant in min^{-1}, k_r is the reaction kinetic constant in mol L^{-1} min^{-1}, t is the reaction time in min, and C_0 is the initial equilibrium concentration.

The results of $Ln(C_0\text{-}C_t)+K_a(C_0\text{-}C_t)]$ vs. t, as shown in Fig. 2 indicate that all Nd^{3+}-TiO_2 catalysts demonstrated significant photocatalytic activity under visible light irradiation, while TiO_2 showed almost no photocatalytic activity. The results in Table 2 showed that the rate of MBT degradation increased initially with the increase of Nd^{3+} content, but decreased while the Nd^{3+} content reached a higher level. It was indicated that the optimal Nd^{3+} dosage is around 0.7% in this experimental condition.

[Fig. 2]
[Table 2]

The values of kinetic parameters, k_{ap} and k_r, are listed in Table 2. It can be seen that 0.7% Nd^{3+}-TiO_2 catalyst achieved the best performance. To better understand the experimental results, the values of k_{ap}, k_r and K_a for 0.7% Nd^{3+}-TiO_2 and TiO_2 are compared. The apparent kinetic constant (k_{ap}) of 0.7% Nd^{3+}-TiO_2 was about 41 times of that of TiO_2, while the adsorption constant (K_a) and reaction kinetic constant (k_r) were 1.7 times and 24 times, respectively.

To investigate the effect of neodymium ion doping on MBT mineralization, the experiment of MBT degradation with an initial DOC concentration of 10.9 mg L^{-1} was carried out for 100 min, in which 7 samples were collected at the time intervals of 0, 10, 20, 30, 50, 70, and 100 min, respectively. The results of DOC concentration are shown in Fig. 3. It was found that the DOC was removed by 12%, 41%, 48%, 52%, and 57% for TiO_2, 0.2%, 0.7%, 1.2%, and 2.0% Nd^{3+}-TiO_2, respectively. In the meantime, to evaluate the conversion of organic sulphur and organic nitrogen during the MBT photocatalytic degradation, a set of tests was carried out in the suspensions with the initial concentrations of MBT = 48.6 mg L^{-1}, organic sulphur = 18.6 mg L^{-1} and organic nitrogen = 4.07 mg L^{-1} for 400 min, in which 7 samples were collected at 0, 80, 160, 200, 260, 320,

and 400 min, respectively in each test for determination of sulphate ion (SO_4^{2-}), ammonium ion (NH_4^+) and nitrate (NO_3^-). The experimental results using 0.7% Nd^{3+}-TiO_2 are shown in Fig. 4. The experiment demonstrated that the concentrations of SO_4^{2-}-S increased from 0 to 12.7 mg L^{-1} and the concentrations of NH_4^+-N increased from 0 to 2.51 mg L^{-1}, while the concentrations of NO_3^--N increased from 0 to 0.75 mg L^{-1} during the MBT photodegradation reaction. The conversion of organic sulphur was achieved by 68%, while the conversion of organic nitrogen was achieved by 80%. The above results indicate that MBT could be significantly mineralized by using Nd^{3+}-TiO_2 under visible light irradiation.

[Fig. 3]

[Fig. 4]

Chemical and Physical Properties

The XRD diffractograms of Nd^{3+}-TiO_2 samples were tested and all samples show a similar pattern of XRD grams, which is dominated by anatase. The relative intensity of 101 peaks decreases with the increase of neodymium ion dosage significantly. The position of 101 peaks also shifted slightly to a lower angle. For the TiO_2, 0.2%, 0.7%, 1.2%, and 2.0% Nd^{3+}-TiO_2 catalysts, the positions of 101 peaks were determined to be at 2θ = 25.34°, 25.22°, 25.32°, 25.32°, and 25.26°, respectively. The decrease of anatase (101) peak indicates that neodymium ion doping may inhibit the phase transformations from amorphous form to anatase in the solid and leads to higher thermal stability. On the basis of XRD data, the crystallite size of the Nd^{3+}-TiO_2 samples was calculated using the Scherer formula and the results are listed in Table 3. The results indicate that the crystallite size decreases significantly, when Nd^{3+} dosage increases from 0 to 0.7%, and then changes slightly, when Nd^{3+} dosage is higher than 0.7%. It may indicate that the neodymium ion doping could hinder the increase of the crystallite size.

In fact, the ionic radium (0.99Å) of Nd^{3+} is larger than that (0.68Å) of Ti^{4+} and it is difficult for Nd^{3+} to really enter the lattice of TiO_2. Therefore, a charge imbalance is actually caused by the titanium entering into the lattice of lanthanide oxide during heat treatment and let Ti^{4+} reduced to Ti^{3+}. Our group had reported that the amount of Ti^{3+} existing on the surface of photocatalysts increased with the increase of lanthanide ion dosage. The ratio of [O]/[Ti] obtained in the XPS analysis on the surface of photocatalysts increased with the increase of lanthanum ion and neodymium ion dosage [29-31]. Shah et al. [32] proposed that Nd^{3+} might reside in the octahedral interstitial site of Nd^{3+}-TiO_2 and the high oxygen affinities of interstitially located neodymium ion effectively create a localized positive charge around Ti and a Ti-O-Nd bond could form. Moreover, the specific surface area of Nd^{3+}-TiO_2 is larger than that of TiO_2, as listed in Table 3.

[Table 3]

UV-VIS DRS of the TiO_2 and Nd^{3+}-TiO_2 catalysts in the range of 200-800 nm were obtained and are shown in Fig. 5. It can be seen while TiO_2 catalyst has no significant absorption in the visible region of more than 400 nm, the Nd^{3+}-TiO_2 catalysts have several optical absorption peaks at 432, 464, 476, 515, 528, 586, 628, 684, and 747 nm. The peak intensity increases with the Nd^{3+} dosage significantly. The positions of these absorption peaks are in accordance with the internal 4*f* transitions observed in corresponding Nd(III) complexes, which give rise to narrow absorption bands quite unlike normal band gap transitions as reported by Machida et al.[33, 34], Ratnakaram et al.[35], Klink et al.[36], Hwang et al.[23], Mathur et al. [37], Xiang et al. [20], Kwag et al.[38], and Ripoll et al.[39]. The above absorption peaks are attributable from the $^4I_{9/2}$ ground state to higher excited states including: $^2P_{1/2}$+$^2D_{5/2}$ (432 nm), $^2D_{3/2}$+$^4G_{11/2}$ (464 nm), $^2G_{9/2}$+$^2K_{15/2}$ (476 nm), $^4G_{9/2}$ (515 nm), $^4G_{7/2}$ (528 nm), $^4G_{5/2}$ (586 nm), $^2H_{11/2}$ (628 nm), $^4F_{9/2}$ (684 nm), and $^4F_{7/2}$+$^4S_{3/2}$ (747 nm). However, the 4*f* electrons of neodymium ion are shielded by the outer-shell 5*s* and 5*p* electrons, which make the Nd^{3+} energy levels independent on their surroundings. Hwang et al.[23] reported that the band gap energy of lanthanide titanates, $(Nd, La, Pr)_2Ti_2O_7$, is highly dependent on the number of lanthanide 4*f* electrons (Nd^{3+} $4f^4 6s^2$; La^{3+} $4f^0 5d^1 6s^2$; and Pr^{3+} $4f^2 6s^2$). This band gap was also observed for lanthanide tantalates ($LnTaO_4$) and layered perovskite tantalates ($RbLnTa_2O_7$)[24, 25]. It was proposed that the corresponding photoexcited process attributed to 4*f* internal atomic transition should be not responsible for photocatalytic reaction, although Ebitani et al.[40] reported that the photoexcited state of lanthanide ion attributed to 4*f*-5*d* transition or *f*- *f* transition could have the capability of transferring their excited energy to other molecules in a gas phase or the absorbed state. In this study, the absorption band edge of Nd^{3+}-TiO_2 catalysts in the range of 200-400 nm shown in Fig. 5 is highly similar to that of TiO_2. This implies that the direct electron transfers from Nd 4*f* to the conduction band could be difficult because of a larger interatomic distance. However, the occupied 4*f* band for Nd_2O_3 lies above the O 2*p* band. Nd 4*f* may interact with the O 2*p* that participates in deriving the conduction band through Ti-O-Nd interactions.

To better understand the interaction and energy transfer between Nd 4*f* and O 2*p* in this study, the PL emission spectra of all samples in both range of 350-700 nm and 1,000-1,600 nm at room temperature are shown in Fig. 6A and C, respectively, while the PL emission spectra in the range of 350-700 nm at 77 K are shown in Fig. 6B. It can be seen that the PL emission intensity of TiO_2 is much higher than that of the Nd^{3+}-TiO_2 samples in the range of 350-450 nm at room temperature and also at 77 K. As shown in Fig. 6A, the PL peaks of TiO_2 and 0.2% Nd^{3+}-TiO_2 at

420 nm are significant and could be attributable to the host emission, but those of 0.7%, 1.2%, and 2.0% Nd^{3+}-TiO_2 decrease gradually. In addition, their PL emission in the range of 450-700 nm presents obviously without sharp peaks owing to the interaction between Nd 4*f* and O 2*p*. To further clearly disclose this interaction, the PL emission was tested at 77 K. Fig. 6B shows clearly that the intensity of PL emission from Nd^{3+}-TiO_2 samples is much lower than that from TiO_2 and some new PL emission peaks appear obviously at 499-504 nm, 539-546 nm, and 596-608 nm, respectively. The relevant data regarding the PL emission peaks are listed in Table 4. The PL emission peaks of TiO_2 at 520 nm and Nd^{3+}-TiO_2 samples at 522 nm might be attributable to the recombination of the host charge carrier. To our best knowledge, it has not been reported that the PL emission peaks at 400-700 nm are attributable to the intra-4*f* shell transition of Nd^{3+} in any materials. Since the *f-f* transitions are fairly insensitive to the conditions of temperature and the surrounding chemical environment, the PL emission peaks in Fig. 6C could be attributable to the intra-4*f* shell transition of Nd^{3+} while the PL emission peaks except that at 522 nm in Fig. 6B might be attributed to the energy transfer between Nd 4*f* and O 2*p*. Fig. 6C shows that the significant PL emission from 0.7%, 1.2%, and 2.0% Nd^{3+}-TiO_2 occurred at 1,100, 1,381, and 1,417 nm, respectively, and the intensity increases with the increase of neodymium ion dosage, while the PL emission from TiO_2 and 0.2% Nd^{3+}-TiO_2 is very weak in the same region. The PL properties of the rare earth ion (Sm^{3+}, Dy^{3+}, Er^{3+}, Tm^{3+}, Eu^{3+}, Tb^{3+}, Pr^{3+})-doped $K_2La_2Ti_3O_{10}$, $KLaNb_2O_7$ and $K_{2-x}H_xTi_2O_5$ with layered perovskite structure have been reported by Kudo et al.[41-43]. Watanabe et al.[44] reported the energy transfer between Nd^{3+} and Si nanocrystals and also the PL peaks at 0.87 eV (1,425 nm), 1.12 eV (1,107 nm), and 1.36 eV (912 nm), corresponding to the intra-4*f* shell transition of Nd^{3+} ($^4F_{3/2}$ to $^4I_{13/2}$, $^4F_{3/2}$ to $^4I_{11/2}$, $^4F_{3/2}$ to $^4I_{9/2}$, respectively). Similarly, Buissette et al.[45] found these peaks at 1,340 nm, 1,060 nm and 880 nm attributable to the intra-4*f* shell transition of Nd^{3+} for YVO_4Nd nanoparticle. Frindell et al.[22] found the 912 nm and 1,060 nm for the 4% Nd^{3+}-doped mesoporous titania thin film. The energy transfer and electron transfer processes between host and guest play a vital role in photocatalytic reaction and should be of particular interest from the viewpoint of the development of new host-guest systems. On the basis of the above results, a valence band structure of Nd^{3+}-TiO_2 catalysts is proposed as illustrated in Fig. 7. It is suggested that electron-hole pairs in Nd^{3+}-TiO_2.could be generated under visible light irradiation. The electron can be excited from the valence band of Nd^{3+}-TiO_2 into Nd 4*f* level when the energy of photon is more than ($E_{Nd4f} - E_v$). Therefore, the photocatalytic excitation of Nd^{3+}-TiO_2 under visible light irradiation is expressed by Equation 1. It should be indicated that the Nd 4*f* levels might play a crucial role in generating electron-hole pairs under visible illumination.

$$Nd^{3+}\text{-}TiO_2 + h\nu \rightarrow e^- + h^+ \quad (1)$$

[Fig. 7]

[Table 4]

Mechanism of the Enhanced Photocatalytic Activity of TiO_2 Catalysts with Neodymium Ion Doping

In general, photocatalytic activity of TiO_2 catalysts depends strongly on several factors such as the adsorption behaviour, the separation of electron-hole pair, and optical properties. The main purpose of current study is to elucidate the effects of neodymium ion doping on the photocatalytic activity of TiO_2 catalysts. Since the effect of neodymium ion doping on the adsorption behaviour of TiO_2 catalysts has been investigated In the above study, the effect of neodymium ion doping on the separation of electron-hole pairs within TiO_2 catalysts can be further discussed. In fact, Wang and his co-workers proved that the separation of electron-hole pairs in lanthanide ion (La^{3+}, Nd^{3+}, Pr^{3+}, Sm^{3+}, or Eu^{3+})-doped TiO_2 structure is more efficient than that in pure TiO_2.[46] Frindell group[22] proposed a model for an energy transfer involving relaxation to defect level first and then to the lanthanide ions in the lanthanide ion-doped TiO_2 catalyst. In this study, the PL emission spectra of Nd^{3+}-TiO_2 catalysts imply an electron transfer from TiO_2 to Nd^{3+} crystal field states. The energy level of crystal field state is the critical information about the electron transfer process. For the Nd^{3+}-TiO_2 catalysts, Nd 4*f* level plays an important role in interfacial charge transfer and elimination of electron-hole recombination. Neodymium ion could act as an effective electron scavenger to trap the conduction band (CB) electrons of TiO_2. In addition, neodymium ions as a Lewis acid, apparently are superior to the oxygen molecule (O_2) in the capability of trapping CB electrons.[47] The electrons trapped in Nd^{3+}/Nd^{2+} sites are subsequently transferred to the surrounding adsorbed O_2. The presence of Nd^{3+} on TiO_2 surface may promote several electron transfer steps as summarized below:

$$TiO_2\ (e^-) + O_2 \rightarrow O_2^- + TiO_2 \quad (2)$$

$$TiO_2\ (e^-) + Nd^{3+} \rightarrow Nd^{2+} + TiO_2 \quad (3)$$

$$Nd^{2+} + O_2 \rightarrow O_2^- + Nd^{3+} \quad (4)$$

$$O_2^{\bullet -} + 2H^+ \rightarrow 2\bullet OH \quad (5)$$

According to the energy level, the photogenerated electrons are permitted to transit from TiO_2 CB to Nd^{3+} ions and Nd^{3+} oxidation state ion can effectively trap the electrons. On the other hand, lanthanide metals have partially filled atomic *d* or *f* shell, the electrons at Ln^{n+} 4*f* orbit could conduct electron-excitation and electron-transition to build up lanthanide ions with a higher valence state by absorbing proper photons energy. Consequently, surrounding Ln^{n+} ions may mutually bond by self-sensitization and form positively charged lanthanide ions cluster $(Ln_p)^{q+}$ ($q > 3p$). This

lanthanide cluster has discrete empty multi-energy levels below the conduction band of crystalline TiO_2. Their presence allows a new electronic transition from the TiO_2 valence band to the empty lanthanide ion cluster energy levels known as a sub-band gap with less energy than TiO_2 valence-conduction band transition as illustrated in Fig. 7.

[FIG. 7]

Conclusions

The Nd^{3+}-TiO_2 catalysts prepared in this study demonstrated significant photocatalytic activity under visible light irradiation to degrade MBT in aqueous solution. The adsorption isotherm experiments confirmed that both the adsorption capacity and the adsorption equilibrium constants of the Nd^{3+}-TiO_2 catalysts increased with the increase of neodymium ion dosage, that might be attributed partially to the increase of the specific surface area for the Nd^{3+}-TiO_2 catalysts and somewhat to the formation of Lewis acid-base complexes between Nd^{3+} and the –SH groups of MBT. The Nd^{3+}-TiO_2 catalysts demonstrated faster MBT photodegradation rates with an optimum dosage of 0.7%. The PL emission spectra results also imply that the electron transfer between TiO_2 and Nd^{3+} should be a vital fact in suppressing the recombination of charge carriers. It is concluded that the mechanisms of the enhancement of photocatalytic activity of Nd^{3+}-TiO_2 for the MBT photocatalytic degradation might be attributed to the improvements of the adsorption ability and also the separation of electron-hole pairs. The experiments also confirmed that MBT in aqueous Nd^{3+}-TiO_2 suspension can be significantly mineralized under visible light irradiation.

Acknowledgement

Authors would like to thank a financial support from The Hong Kong Polytechnic University as the Postdoctoral Fellowship Grant (Project No.: G-YW69/02).

References

1. H. De Wever, H. Verachtert, *Appl. Microbiol. Biotechnol.* **1994,** 42, 623.
2. O. Fiehn, G. Wegener, J. Jochimsen, M. Jekel, *Wat. Res.* **1998,** 32, 1075.
3. M. H. Habibi, S. Tangestaninejad, B. Yadollahi, *Appl. Catal. B* **2001,** 33, 57.
4. M. R. Hoffmann, S. T. Martin, W. Choi, D. W. Bahnemann, *Chem. Rev.* **1995,** 95, 69.
5. J. G. Yu, J. C. Yu, B. Cheng, X. J. Zhao. *J. Sol-Gel Sci. Technol.* **2002,** 24, 39.
6. H. Kato, A. Kudo, *J. Phys. Chem. B.* **2002,** 106*,* 5029.
7. T. Umebayashi, T. Yamaki, H. Itoh and K. Asai, *Journal of Physics and Chemistry of Solids* **2002,** 63, 1909.
8. A. Yamakata, T. Ishibashi, H. Onishi, *J. Phys. Chem. B* **2001,** 105, 7258.

9. J. L. Gole, J. D. Stout, C. Burda, Y. Lou, X. Chen, *J. Phys. Chem. B.* **2004,** 108, 1230.
10. T. Sano, N. Negishi, K. Koike, K. Takeuchi, S. Matsuzawa, J. Mater. Chem. **2004,** 14, 380.
11. W. Zhao, W. Ma, C. Chen, J. Zhao, Z. Shuai, *J. Am. Chem. Soc.* **2004,** 126, 4782.
12. T. Ohno, M. Akiyoshi, T. Umebayashi, K. Asai, T. Mitsui and M. Matsumura. *Appl. Catal. A: Gen.* **2004,** 265, 115.
13. M. Miyauchi, A. Nakajima, T. Watanabe, K. Hashimoto, *Chem. Mater.* **2002,** 14, 4714.
14. X. Z. Li, F. B. Li, C. L. Yang, W. K. Ge, *J. Photochem. Photobiol. A: Chem.* **2001,** 141, 209.
15. M. R. Dhananjeyan, E. Mielczarski, K.R. Thampi, P. Buffat, M. Bensimon, A. Kulik, J. Mielczarski, J. Kiwi, *J. Phys. Chem. B* **2001,** 105, 12046.
16. B. M. Reddy, P. M. Sreekanth, E. P. Reddy, Y. Yamada, Q. Xu, H. Sakurai, T. Kobayashi, *J. Phys. Chem. B* **2002,** 106, 5695.
17. Y. A. Cao, X. T. Zhang, W. S. Yang, H. Du, Y. B. Bai, T. J. Li, J. N. Yao, *Chem. Mater.* **2000,** 12, 3445.
18. S. Ikeda, N. Sugiyama, B. Pal, G. Marcí, L. Palmisano, H. Noguchi, K. Uosaki, B. Ohtani, *Phys. Chem. Chem. Phys.* **2001,** 3, 267.
19. Y. B. Xie, C. W. Yuan, Appl. Surf. Sci. **2004,** 221, 17.
20. Q. Xiang, Y. Zhou, Y. L. Lam, Y. C. Chan, C. H. Kam, B. S. H. Ooi, X. Zhang, S. Buddhudu, *Materials Research Bulletin* **2000,** 35, 1571.
21. D. D. Jia, R. S. Meltzer. W. M. Yen, *Phys. Rev. B* **2002,** 65, 235116.
22. K. L. Frindell, M. H. Bartl, M. R. Robinson, G. C. Bazan, A. Popitsch, G. D. Stucky, *J. Solid State Chem.* **2003,** 172, 81.
23. D. W. Hwang, J. S. Lee, W. Li, S. H. Oh, *J. Phys. Chem. B* **2003,** 107, 4963.
24. M. Machida, S. Murakami, T. Kijima, S. Matsushima, M. Arai, *J. Phys. Chem. B.* **2001,** 105, 3289.
25. M. Machida, K. Miyazaki, S. Matsushima, M. Arai, *J. Mater. Chem.* **2003,** 13, 1433.
26. Z. G. Zou, J. H. Ye, H. Arakawa, *J. Phys. Chem. B* **2002,** 106, 517.
27. X. Z. Li, H. Liu, L. F. Cheng, H. J. Tong, *Environ. Sci. & Technol.* **2003,** 37, 3989.
28. K. T. Ranjit, I. Willner, S. H.Bossmann, A. M. Braun, *Environ. Sci. Technol.* **2001,** 35, 1544.
29. F. B. Li, X. Z. Li, M. F. Hou, K. W. Cheah, W. C. H. Choy. *Appl. Catal. A* **2005,** 285, 181.
30. F. B. Li, X. Z. Li and M. F. Hou. *Appl. Catal. B: Environ.* **2004,** 48, 185-194.
31. M. F. Hou, F. B. Li, R. F. Li, H. F. Wan, G. Y. Zhou, K. C. Xie. *J. Rare Earths,* **2004,** 22,542.
32. S. I. Shah, W. Li, C.-P. Huang, O. Jung, C. Ni, *Proc. Nat. Acad. Sci.* **2002,** 99, 6482.
33. M. Machida, J.-i. Yabunaka, T. Kijima, *Chem. Mater.* **2000,** 12, 812.
34. M. Machida, J.-i. Yabunaka, T.Kijima, *Chem. Commu.* **1999,** 1939.
35. Y. C. Ratnakaram, S. Buddudu, *Solid State Commum.* **1996,** 97, 651.
36. S. I. Klink, L. Grave, D. N. Reinhoudt, F. Veggel, M. H. V. Werts, F. A. J. Geurts, J. W. Hofstraat, *J. Phys. Chem. A* **2000,** 104, 5457.
37. S. Mathur, M. Veith, H. Shen, S. Hufner, M. H. Jilavi, *Chem. Mater.* **2002,** 14, 568.
38. G. Kwag, H. Lee, S. Kim, *Macromolecules* **2001,** 34, 5367.

39. J. Ripoll, L. E. Bausa, C. Terrile, J. G. Sole, F. Diaz, *Journal of Luminescence* **1997,** 72-74, 253.
40. K. Ebitani, Y. Hirano, A. Morikawa, *J. Cata.* **1995,** 157, 262.
41. A. Kudo, T. Sakata, *J. Phys. Chem.* **1995,** 99, 15963.
42. A. Kudo, *Chem. Mater.* **1997,** 9, 664.
43. A. Kudo, E. Kaneko, *Chem. Commun.* **1997,** 349.
44. K. Watanabe, H. Tamaoka, M. Fujii, K. Moriwaki, S. Hayashi, *Physica E,* **2002,** 13, 1038.
45. V. Buissette, A. Huignard, T. Gacoin, J. -P. Boilot, P. Aschehoug, B. Viana, *Surface Science* **2003,** 532-535, 444.
46. Y. Q. Wang, H. M. Cheng, Y. Z. Hao, J. M. Ma, W. H. Li, S. M. Cai, *J. Mater. Sci. Lett.* **1999,** 18, 127.
47. Y. B. Xie, C. W. Yuan, *Appl. Catal. B: Environ.* **2003,** 46, 251.

Table 1: The saturated adsorption amount (Γ_{max}) and adsorption equilibrium constant (K_a)

Photocatalyst	Γ_{max} (10^{-6}mol g^{-1})	K_a (L mol^{-1})	Correlation coefficient, R^2
TiO_2	8.91	338	0.9918
0.2%Nd^{3+}-TiO_2	12.5	509	0.9949
0.7%Nd^{3+}-TiO_2	13.1	580	0.9920
1.2%Nd^{3+}-TiO_2	13.5	596	0.9914
2.0%Nd^{3+}-TiO_2	14.1	586	0.9892

Table 2: The kinetic parameters of MBT photodegradation with an initial concentration of 0.13 mM

The photo-catalysts	The apparent reaction kinetic constant, k_{ap}/min^{-1}	The kinetic constants, k_r/ 10^{-6}mol L^{-1} min^{-1}	The relative coefficient, R^2
TiO_2	0.0015	0.44	0.9815
0.2%Nd^{3+}-TiO_2	0.0336	6.61	0.9990
0.7%Nd^{3+}-TiO_2	0.0616	10.6	0.9983
1.2%Nd^{3+}-TiO_2	0.0396	6.66	0.9984
2.0%Nd^{3+}-TiO_2	0.0359	6.12	0.9980

Table 3: The crystal size (D), crystal composition, specific surface area, and the position of 101 peak of TiO_2 and Nd^{3+}-TiO_2catalysts

Nd/Ti (mol/mol)	0	0.2	0.7	1.2	2.0
Crystal pattern	Anatase	Anatase	Anatase	Anatase	Anatase
Crystal size (nm)	32.9	25.8	19.2	19.8	17.8
Specific surface area (m^2 g^{-1})	43.29	67.28	71.25	78.54	90.91
The position of 101 peak (°)	25.34	25.22	25.32	25.32	25.26

Table 4: Photoluminescence emission from the TiO_2 and Nd^{3+}-TiO_2 catalysts in the range of 350 - 700 nm at 77 K

Photocatalysts	Peak 1	Peak 2	Peak 3	Peak 4
TiO_2	520	\	\	\
0.7%Nd^{3+}-TiO_2	522	504	539	596
1.2%Nd^{3+}-TiO_2	522	502	542	608
2.0%Nd^{3+}-TiO_2	522	499	546	608

List of figure captions

Fig. 1: The saturated adsorption amounts (Γ_{max}) of the TiO_2 and Nd^{3+}-TiO_2 catalysts vs. equilibrium concentration (C_e)

Fig. 2: The photocatalytic kinetic of MBT degradation, $[Ln(C_0\text{-}C_t)+K_a(C_0\text{-}C_t)]$ vs reaction time with an initial concentration of 0.13 mM under visible light irradiation

Fig. 3: The DOC removal in MBT photocatalytic degradation using different catalysts under visible light irradiation

Fig. 4: The concentration of the final products from the MBT degradation vs. reaction time

Fig. 5: The UV-visible diffuse reflectance spectra (DRS) of TiO_2 and Nd^{3+}-TiO_2 catalysts

Fig. 6: The photoluminescence emission spectra of TiO_2 and Nd^{3+}-TiO_2 powders at room temperature and 77 K

Fig. 7: The proposed valence band structure of Nd^{3+}-TiO_2 and the mechanisms of photoresponse under visible light and photogenerated electron transfer.

Fig. 1

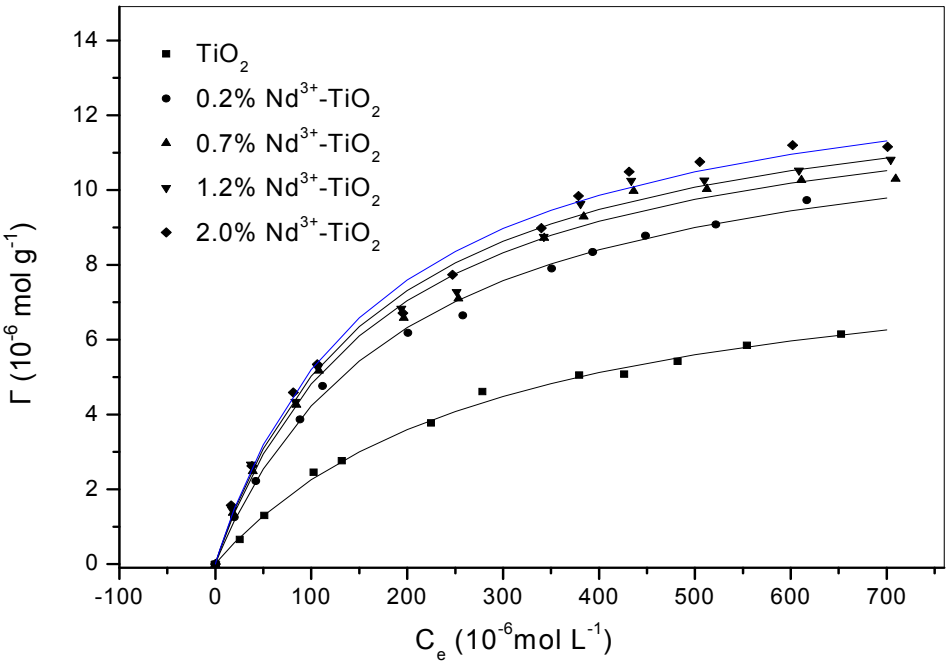
TiO2
0.2% Nd3+-TiO2
0.7% Nd3+-TiO2
1.2% Nd3+-TiO2
2.0% Nd3+-TiO2
Γ (10-6 mol g-1)
Ce (10-6mol L-1)
0
2
4
6
8
10
12
14
-100
0
100
200
300
400
500
600
700

Fig. 2

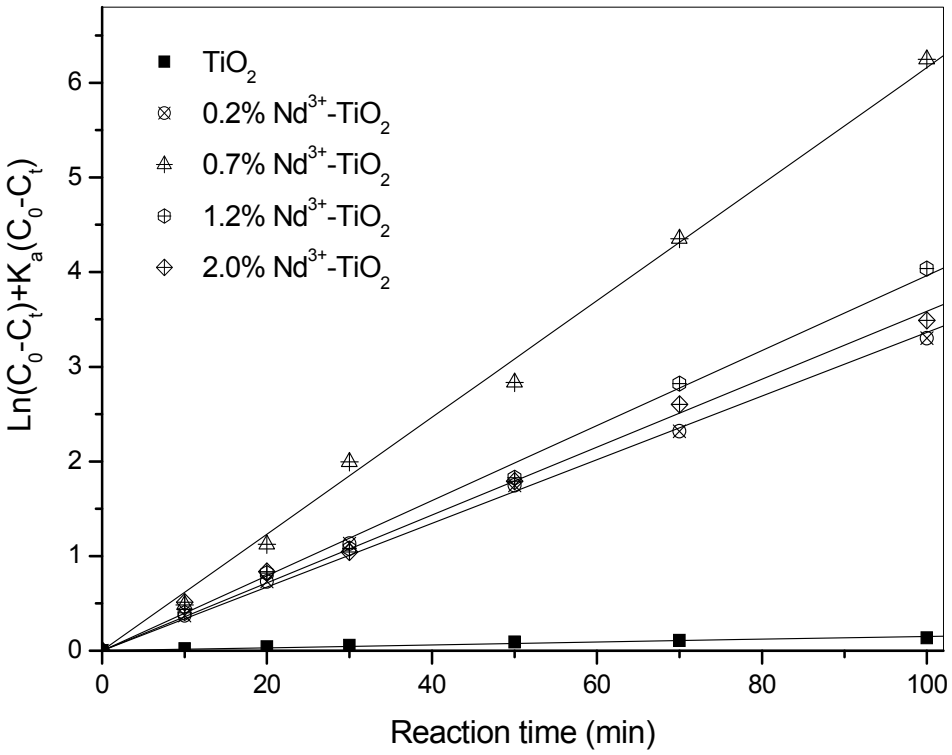
TiO2
0.2% Nd3+-TiO2
0.7% Nd3+-TiO2
1.2% Nd3+-TiO2
2.0% Nd3+-TiO2
Ln(C0-Ct)+Ka(C0-Ct)
Reaction time (min)
0
1
2
3
4
5
6
0
20
40
60
80
100

Fig. 3

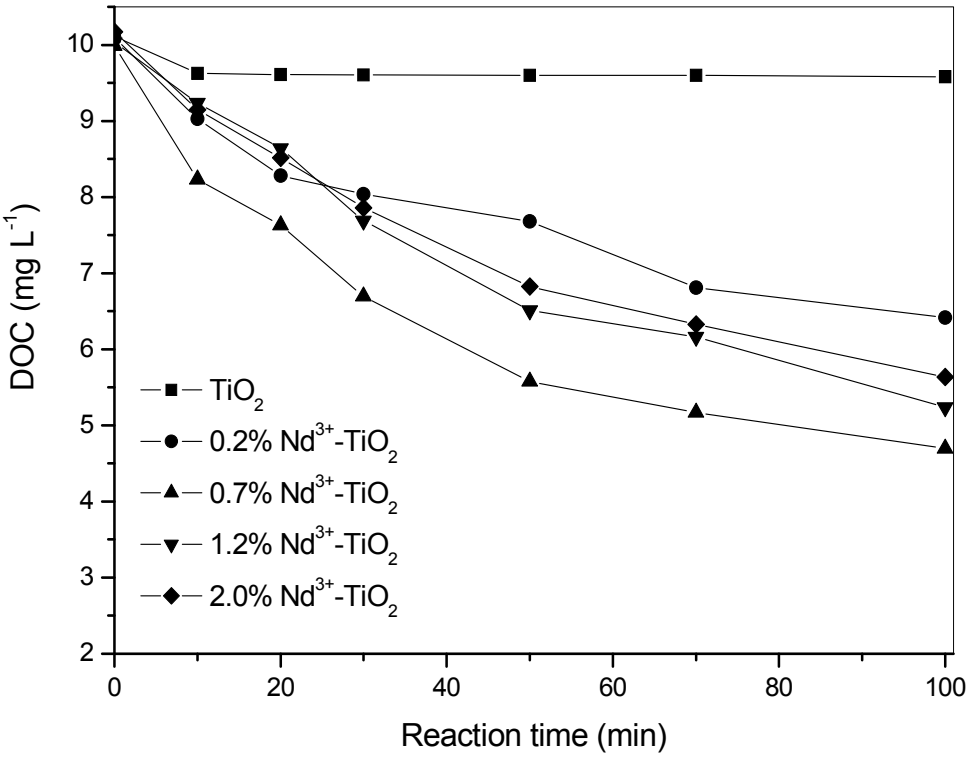
DOC (mg L-1)
Reaction time (min)
TiO2
0.2% Nd3+-TiO2
0.7% Nd3+-TiO2
1.2% Nd3+-TiO2
2.0% Nd3+-TiO2

Fig. 4

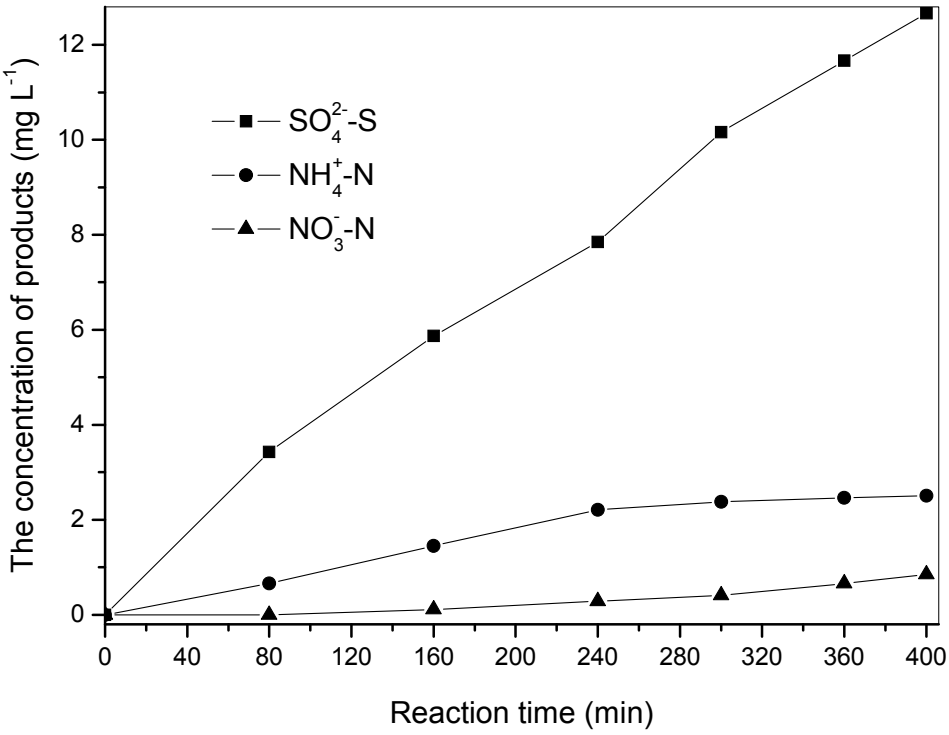
The concentration of products (mg L-1)
Reaction time (min)
SO42--S
NH4+-N
NO3--N
0
2
4
6
8
10
12
0
40
80
120
160
200
240
280
320
360
400

Fig. 5

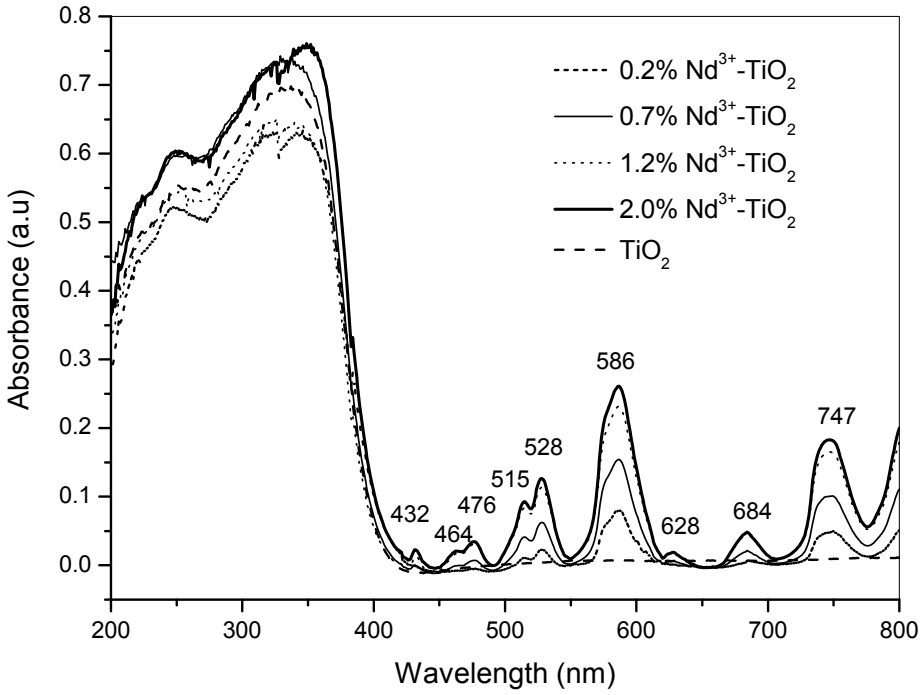
0.2% Nd3+-TiO2
0.7% Nd3+-TiO2
1.2% Nd3+-TiO2
2.0% Nd3+-TiO2
TiO2
Absorbance (a.u)
Wavelength (nm)
0.0
0.1
0.2
0.3
0.4
0.5
0.6
0.7
0.8
200
300
400
500
600
700
800
432
464
476
515
528
586
628
684
747

Fig. 6

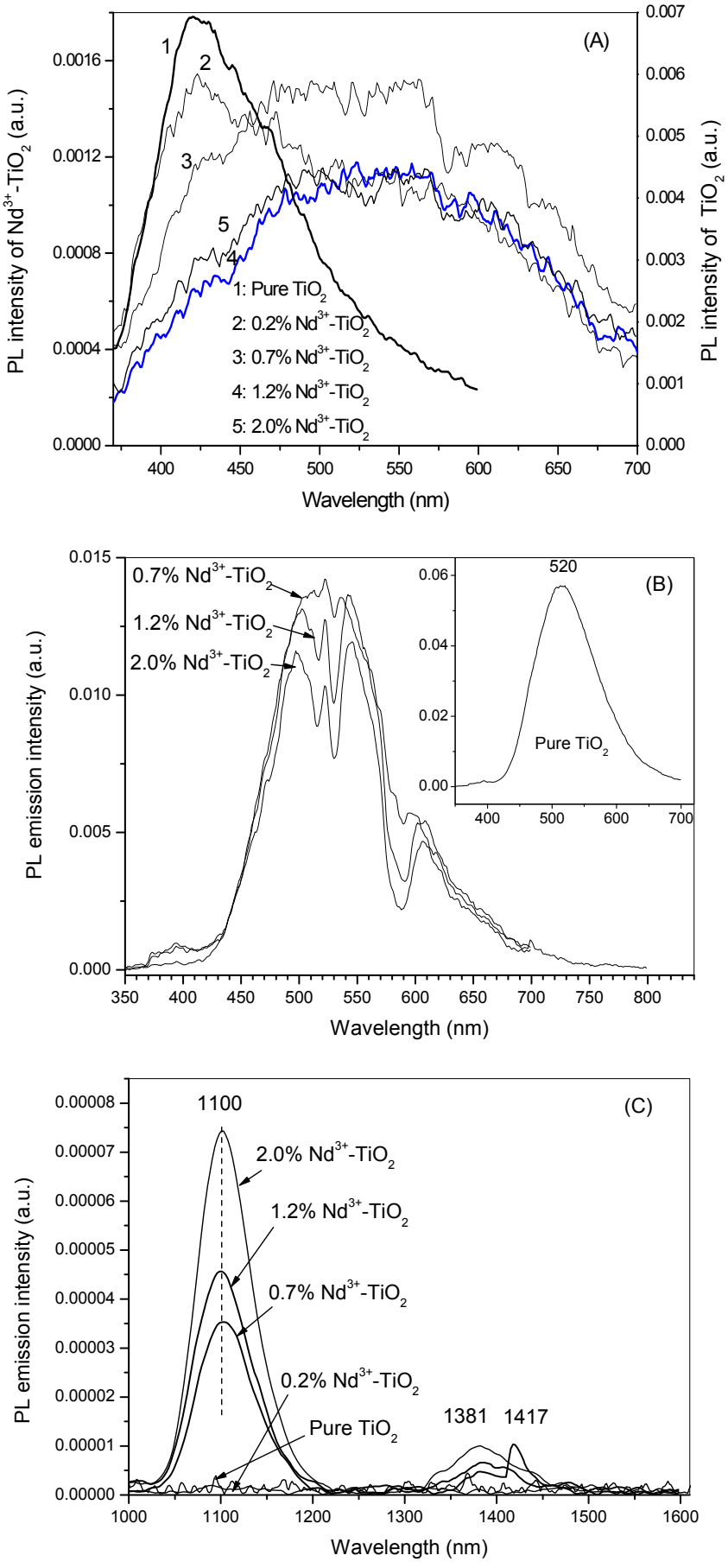
(A)
PL intensity of Nd3+-TiO2 (a.u.)
PL intensity of TiO2 (a.u.)
Wavelength (nm)
1: Pure TiO2
2: 0.2% Nd3+-TiO2
3: 0.7% Nd3+-TiO2
4: 1.2% Nd3+-TiO2
5: 2.0% Nd3+-TiO2
(B)
PL emission intensity (a.u.)
0.7% Nd3+-TiO2
1.2% Nd3+-TiO2
2.0% Nd3+-TiO2
520
Pure TiO2
Wavelength (nm)
(C)
PL emission intensity (a.u.)
1100
2.0% Nd3+-TiO2
1.2% Nd3+-TiO2
0.7% Nd3+-TiO2
0.2% Nd3+-TiO2
Pure TiO2
1381
1417
Wavelength (nm)

Fig. 7

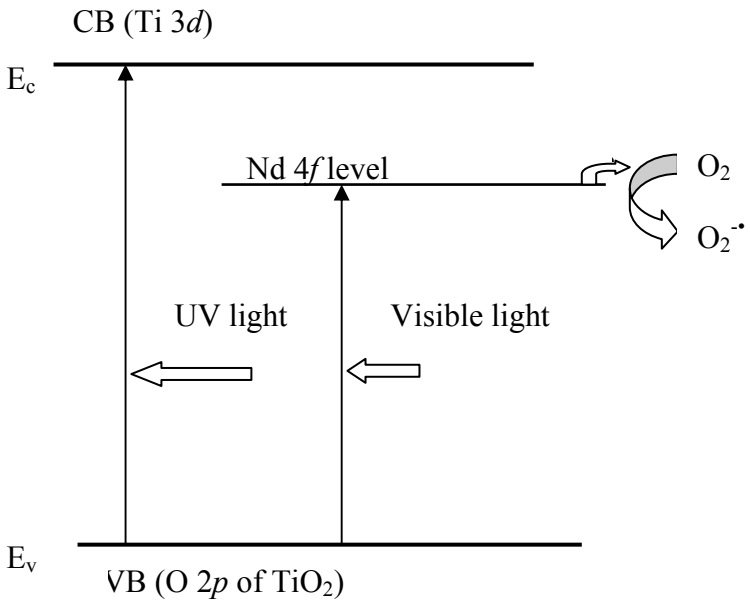
CB (Ti 3d)
Ec
Nd 4f level
O2
O2-•
UV light
Visible light
Ev
VB (O 2p of TiO2)